Experimental verifications on an effective model for photonic coupling

Meng Qiu,[1] Shiyi Xiao,[1] Qiong He,[1,2] Shulin Sun,[3] and Lei Zhou[1,2,*]

[1]*State Key Laboratory of Surface Physics and Key Laboratory of Micro and Nano Photonic Structures (Ministry of Education), Fudan University, Shanghai 200433, China*

[2]*Collaborative Innovation Center of Advanced Microstructures, Nanjing 210093, China*

[3]*Department of Optical Science and Engineering and Shanghai Engineering Research Center of Ultra-Precision Optical Manufacturing, Fudan University, Shanghai 200433, China*

**Corresponding author: phzhou@fudan.edu.cn*

Received October 27, 2014; accepted December 4, 2014;
posted December 16, 2014 (Doc. ID 225787); published January 14, 2015

Combining near-field measurements with coupled-mode-theory analyses, we unambiguously identify all resonant modes in coupled systems containing two photonic resonators. Based on this technique, we perform extensive microwave experiments to study how the inter-resonator coupling varies against various configurational parameters. Our experimental results quantitatively verify a previously established effective model for photonic coupling, and highlight the importance of quadrupole terms in certain situations. © 2015 Optical Society of America

OCIS codes: (230.4555) Coupled resonators; (230.5750) Resonators.
http://dx.doi.org/10.1364/OL.40.000272

Couplings between photonic resonators have drawn much attention in photonic research recently [1–19]. Available experiments have shown rich and intriguing phenomena, which were usually explained by full-wave simulations [1–5]. However, while simulations can accurately repeat most experimental findings, the physics behind the observed effects cannot be understood in a simple way. Some simplified models were adopted to explain certain physical effects observed experimentally, but they are either incomplete [6–11] (e.g., only considering electric-dipolar interactions) and/or derived based on some approximations [12–14]. Very recently, we derived an effective model for photonic resonance couplings from a tight-binding formalism based on full Maxwell's equations [20]. In particular, the coupling between two photonic resonators, defined as the frequency splitting between the symmetrical (f_+) and anti-symmetrical modes (f_-), is expressed generally as [20]

$$\Delta f = f_+ - f_- = t_{pp} + t_{mm} + t_{pp}^{\mathrm{rad}} + t_{pm}, \qquad (1)$$

which includes not only the dipolar interactions between electric (t_{pp}) and magnetic dipoles (t_{mm}), but also a radiation correction term (t_{pp}^{rad}) and the electric-magnetic cross-interaction term (t_{pm}) [20]. This model has considered *all* interactions between electromagnetic (EM) dipoles possessed by two resonators, and was verified by full wave simulations in different frequency domains under various configurations [20]. Obviously, using such a model can not only save much computational time in studying complicated coupled systems, but also yield deep physical understandings on such problems. However, so far no experimental verifications on this model appear.

In this report, we perform extensive microwave experiments to verify this model using split-ring-based EM resonators. Combining near-field measurements with coupled-mode-theory (CMT) analyses, we can unambiguously identify both the symmetrical and anti-symmetrical modes of a coupled system, so that the resonance coupling behaviors can be systematically studied. Our experiments verify the effective model in most situations, and reveal the importance of quadrupole contributions in certain cases.

Figure 1(a) schematically depicts our experimental setup. To detect the resonance modes of a given system, we use a dipole antenna (defined as port 1) to excite the coupled system and a monopole antenna (defined as port 2) to detect its response. Both antennas can be placed at different local positions on the surfaces of two resonators, and are connected to a network analyzer (Agilent E8362 C PNA). We first do a benchmark experiment to study the response of a single split-ring-resonator (SRR). The SRR is made by 75-μm-thick copper film with inner/outer radii fixed as 8 and 9.6 mm, placed on a 2-mm-thick FR-4 substrate ($\varepsilon_r = 3.9$). The gap of the

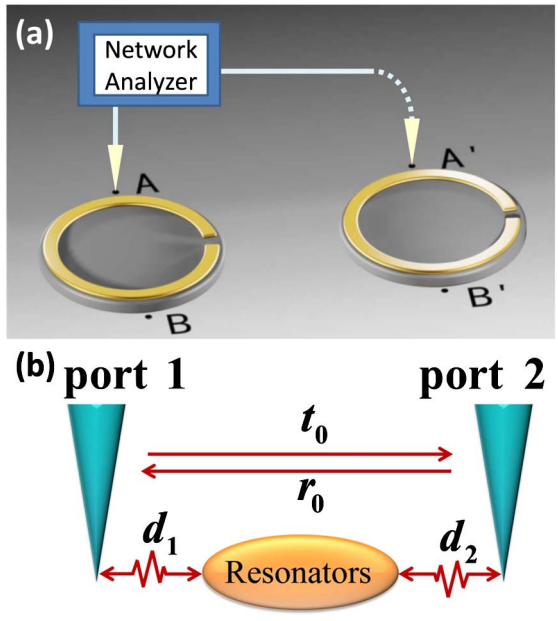

Fig. 1. (a) Schematics of our experimental setup. (b) Pictorial representation of our experiment in coupled-mode theory.

 © 2015 Optical Society of America

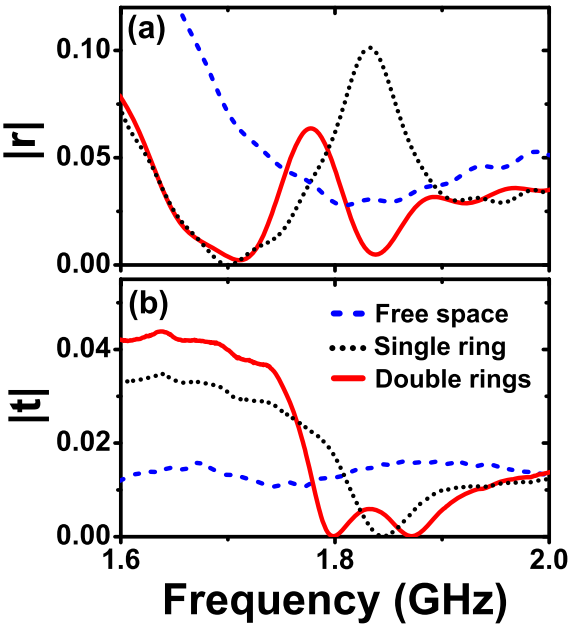

Fig. 2. Measured (a) r and (b) t spectra when there are no SRRs, only one SRR, and two SRRs separated by a distance 23 mm.

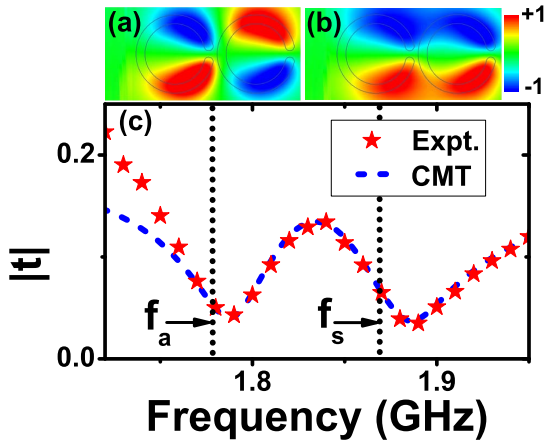

Fig. 3. Normalized Re(E_z) patterns measured by near-field scanning at frequencies (a) f_a and (b) f_s. (c) Transmission spectra for the coupled SRR system obtained by experimental measurements and fitting based on the CMT. Vertical dotted lines denote the resonance frequencies retrieved from the CMT.

SRR is 1.2 mm. Putting the source and receiver antennas at points A and B [see Fig. 1(a)], respectively, we measure the transmission ($t = |S_{21}|$) and reflection ($r = |S_{11}|$) spectra and then plot the results in Fig. 2 (black dotted lines). Compared to the spectra measured without any SRR (blue dashed lines), a peak (dip) appears at ~1.84 GHz in the reflection (transmission) spectra measured with a SRR, implying the existence of a resonance mode. When we add another identical SRR to form a coupled system [see Fig. 1(a)] and repeat the measurements, we find two peaks (dips) in the reflection (transmission) spectra (red solid lines), apparently caused by the resonance coupling.

To identify the symmetries of the modes, we perform near-field scanning experiments to map the Re(E_z) field distributions on a plane 0.5 mm above the SRR, at frequencies near two resonances. Figures 3(a)–3(b) shows clearly that the lower (higher) mode is the anti-symmetrical (symmetrical) mode. However, we find it difficult to unambiguously identify the precise positions of these two modes just from the spectra, which are crucial to test the model Eq. (1). For example, Fig. 2 shows that the peaks in the r spectrum do not match precisely with the dips in the t spectrum, and also the high-frequency peak in the r spectrum is quite obscure. In addition, the dips in the spectrum may significantly shift in positions or even disappear when we change the receiver to a different detection point.

This problem can be remedied by carefully analyzing the experimental data with the CMT. As shown in Fig. 1(b), the signal received by port 2 contains not only that directly radiated from port 1, but also that radiated from the resonant system that is excited by port 1. Let r_0 and t_0 denote the amplitudes of transmitted and reflected signals contributed by the direct channel, an elegant CMT analysis [21] shows that the total transmission can be generally written as

$$t = t_0 + \frac{W_a d_{1s} d_{2s} + W_s d_{1a} d_{2a} + W_s W_a X (d_{1s} d_{2a} + d_{2s} d_{1a})}{W_s W_a - X^2}, \tag{2}$$

where $W_i = i(\omega - \omega_i) + \Gamma_i + \Gamma_i'$ with ω_i, Γ_i and Γ_i' denoting the resonance frequency, the damping caused by radiations to two ports, and the damping caused by absorption and radiations to the far field. Here $i = s, a$ define the symmetrical (s) or anti-symmetrical (a) mode. d_{1i} and d_{2i} ($i = s, a$) denote the couplings between the i-th mode and the two ports, and X describes the interactions between two resonant modes. We note that in the limit of $X = 0$, Eq. (2) reduces to $t = t_0 + d_{1s} d_{2s}/W_s + d_{1a} d_{2a}/W_a$, describing the responses of two *independent* oscillators. X and Γ_i are not independent parameters, since $X = -(d_{1s}^* d_{1a} + d_{2s}^* d_{2a})/2$ and $\Gamma_i = (|d_{1i}|^2 + |d_{2i}|^2)/2$ according to the CMT [22]. Symmetry consideration further shows that $d_{1i} = d_{2i} = d_i$. Finally, phases of d_1 and d_2 are tied with the local external field at the position where the SRR is placed, which are determined by t_0 and r_0 based on an elegant time-reversal argument [21]. Therefore, we only have 6 free parameters in Eq. (2), which are ω_i, $|d_i| = \Gamma_i$, and Γ_i' ($i = s, a$) [22]. We note that similar results can be obtained via analyzing the reflection spectrum based on the CMT.

Dashed lines in Fig. 3(c) are the best fitted CMT spectra with parameters given by $\Gamma_a = \Gamma_s = 0.227$, $\Gamma_a' = 0.054$, $\Gamma_s' = 0.077$, $f_a = 1.78$, $f_s = 1.87$, all in units of GHz. We note that those resonance modes retrieved from the CMT analyses, labeled by two dotted vertical lines in Fig. 3, are *neither* at the peak *nor* at the dip positions of the spectra. Such deviation is an intrinsic property of the Fano spectra involving low-Q resonant modes [21,22], and can be very significant in certain cases (say, when two modes are close to each other), so that a CMT analysis is particularly important to get physically meaningful results in such problems.

Having established a reliable approach to determine the precise mode positions, we now verify the effective model Eq. (1) by performing a series of experiments. We

first verify the magnetic part of the effective model by adopting two broad-side coupled SRRs (BC-SRR) that exhibit *pure* magnetic dipoles $\vec{m}$ at their lowest resonances [23]. Our BC-SRR contains two copper split rings printed on two sides of a 0.4-mm-thick substrate (with $\varepsilon_r = 4.4$), each having inner/outer radii 4 mm and 4.8 mm, and a 0.2-mm gap. We first experimentally identify that the lowest resonance mode of a single BC-SRR is at $f_0 = 1.39$ GHz. We next arrange the two BC-SRRs parallel with each other but with their centers separated by a distance d (see inset to Fig. 4), and then experimentally determine the mode splitting Δf in different cases. Solid stars in Fig. 4 describe how the measured $\Delta f/f_0$ varies against d and θ, where θ is the angle between $\vec{m}$ and $\vec{d}$.

On the other hand, for such a configuration, the effective mode [20] gives that

$$\Delta f/f_0 \approx \frac{\mu_0}{4\pi\langle\Phi|\Phi\rangle}\cdot\frac{(1-3\cos^2\theta)|\vec{m}|^2}{d^3}, \tag{3}$$

where $\langle\Phi|\Phi\rangle$ is a normalization constant. Solid lines in Fig. 4 are the results calculated from such an effective model [24]. We also perform FDTD simulations on realistic systems to study the resonance mode splitting, and depict the results in Fig. 4 as open squares. The measured data agree well with both FDTD simulations on realistic systems and the effective model in most cases, which verify the magnetic part of our model Eq. (1). Slight discrepancies exist between the model and experiment in the small-d region, implying that the dipolar interaction might be insufficient.

To justify the remaining terms in the effective model, we next consider a more complex system containing two single-ring SRRs. Such particle exhibits both electric and magnetic dipole moments at its lowest resonance, so that the coupling between two such particles involves *all* four terms in the effective model Eq. (1). The single-ring SRRs adopted here are the same as those studied in Fig. 2. As shown in Figs. 5(b) and (c), we place two SRRs on the same plane and rotate one of the particles to change the inter-particle configurations, and then experimentally determine the resulting mode-splitting. The difference between two configurations is that the gaps of two SRRs are on the same sides in Fig. 5(b) but on the opposite sides in Fig. 5(c).

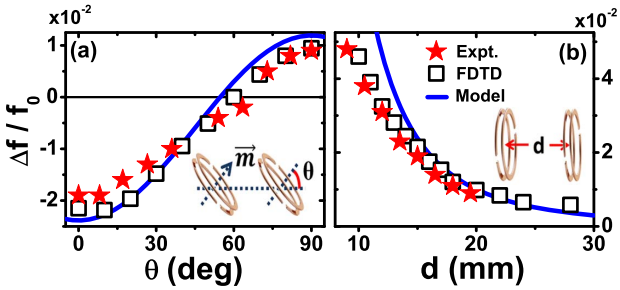

Fig. 4. Resonance frequency splitting versus (a) the orientation angle θ and (b) the inter-particle distance d for the coupled BC-SRR systems, obtained by experiments (red stars), FDTD simulations (black squares), and the model calculations (blue lines). Here we set $d = 15$ mm in (a) and $\theta = 0°$ in (b).

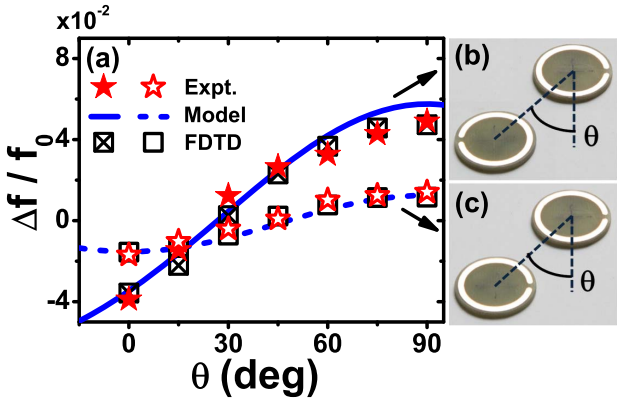

Fig. 5. (a) Resonance frequency splitting versus the orientation angle θ for coupled single-SRR systems with two configurations [sample pictures shown in (b) and (c)], obtained by experiments, FDTD simulations, and the model calculations. Here the inter-particle distances are fixed as 26 mm in both configurations.

Solid stars in Fig. 5 are the experimentally measured $\Delta f/f_0$ versus the orientation angle θ for two configurations, both with inter-SRR distance fixed as 26 mm. While the measured Δf increasingly depend on θ in both cases, the two $\Delta f \sim \theta$ curves intersect at an angle $\theta \approx 15°$. Such an intriguing phenomenon has already been predicted by our effective model [20]. Specifically, according to the effective model, we get that

$$\Delta f/f_0 \approx \frac{1}{4\pi\langle\Phi|\Phi\rangle d^3}\left\{\begin{array}{l}\frac{|\vec{p}|^2}{\varepsilon_0}\cdot\left[\left(1-\frac{(kd)^2}{2}\right)-\left(3+\frac{(kd)^2}{2}\right)\cos^2\theta\right] \\ \pm\left(\frac{\omega_0|\vec{p}||\vec{m}|d}{\varepsilon_0 c^2}\sin\theta-\mu_0|\vec{m}|^2\right)\end{array}\right\}, \tag{4}$$

with sign "±" standing for the configurations shown in Figs. 5(b) and (c), respectively, and k the free-space wave-vector. Such a difference in Δf [Eq. (4)] is caused by different orientations of $\vec{m}$ in the SRRs under two configurations [20]. Solid lines in Fig. 5(a) depict the calculated results based on Eq. (4). Again, FDTD simulations on realistic structures are shown in the same figure for comparison. The agreements between experiment and model in two distinct systems are remarkable, which are the direct evidences to verify our effective model.

Finally, we experimentally test the validity region of our effective model by considering one particular configuration—the gaps of two SRRs are face to face as shown in the inset to Fig. 6. We perform a series of experiments to measure how $\Delta f/f_0$ varies against θ and d for this particular configuration and depict the results in Fig. 6. We find that the experimental data shows non-negligible deviations from the effective model [Eq. (4)], especially in the cases of $\theta \to 90°$ and $d \to 0$. While the CMT might be inaccurate in studying strong coupled systems, such deviations also suggest that the effective model, containing only terms related to EM *dipole* moments, might become insufficient. In fact, in the cases of $\theta \to 90°$ or $d \to 0$, near-field couplings between electric charges accumulated around two gaps are so strong that higher order multipolar interactions must be taken into account. According to Ref. [20], the leading

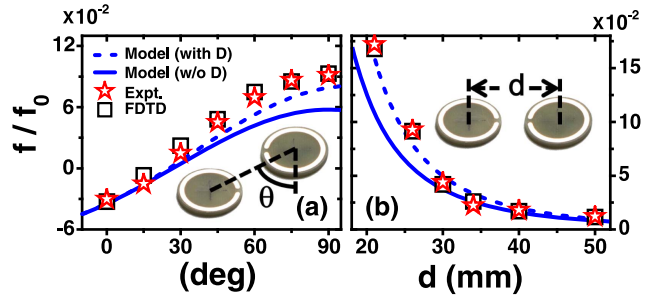

Fig. 6. Resonance frequency splitting versus (a) θ (b) the interparticle distance d for the coupled SRR systems, obtained by experiments, FDTD simulations and calculations based on the effective model with or without quadrupole corrections. Insets show the sample pictures and we set $d = 26$ mm in (a).

correction to the effective model [Eq. (1)] is the interaction between the dipole moment $\vec{p}_1$ in one SRR and the quadrupole moment in another, given by

$$t_{pD}^{(E)} = \frac{f_0}{8\pi\varepsilon_0\langle\Phi|\Phi\rangle} \times \left[\frac{-2\overleftrightarrow{D}_2{:}\vec{p}_1^{\,*}\hat{d} + 5(\overleftrightarrow{D}_2{:}\hat{d}\,\hat{d})(\vec{p}_1^{\,*}\cdot\hat{d}) - (\overleftrightarrow{D}_2{:}\overleftrightarrow{I})(\vec{p}_1^{\,*}\cdot\hat{d})}{d^4}\right]. \quad (5)$$

When such a correction is included, the agreement between experiment and model has been significantly improved, as shown by the dashed lines in Fig. 6.

To summarize, we performed a series of microwave experiments on SRR-based resonators to verify an effective model for photonic coupling. Our experiments justified the model in most cases, and show that it becomes insufficient in certain situations where higher-order corrections must be included.

This work was supported by National Natural Science Foundation of China (Nos. 11474057, 11174055, 11204040, and 11404063), Ministry of Education of China (Grant No. B06011), and the Shanghai Science and Technology Committee (Grant No. 14PJ1401200).

References and Note

1. M. Rycenga, C. M. Cobley, J. Zeng, W. Li, C. H. Moran, Q. Zhang, D. Qin, and Y. Xia, Chem. Rev. **111**, 3669 (2011).
2. N. J. Halas, S. Lal, W. S. Chang, S. Link, and P. Nordlander, Chem. Rev. **111**, 3913 (2011).
3. E. Ozbay, Science **311**, 189 (2006).
4. J. F. Zhou, T. Koschny, M. Kafesaki, and C. M. Soukoulis, Phys. Rev. B **80**, 035109 (2009).
5. K. D. Ko, A. Kumar, K. H. Fung, R. Ambekar, G. L. Liu, N. X. Fang, and K. C. Toussaint, Nano Lett. **11**, 61 (2011).
6. T. J. Davis, K. C. Vernon, and D. E. Gómez, Phys. Rev. B **79**, 155423 (2009).
7. T. J. Davis, D. E. Gomez, and K. C. Vernon, Nano Lett. **10**, 2618 (2010).
8. T. J. Davis, M. Hentschel, N. Liu, and H. Giessen, ACS Nano **6**, 1291 (2012).
9. J. Zuloaga, E. Prodan, and P. Nordlander, Nano Lett. **9**, 887 (2009).
10. P. Nordlander, C. Oubre, E. Prodan, K. Li, and M. Stockman, Nano Lett. **4**, 899 (2004).
11. M. L. Brongersma, J. W. Hartman, and H. A. Atwater, Phys. Rev. B **62**, R16356 (2000).
12. N. Liu, H. Liu, S. N. Zhu, and H. Giessen, Nat. Photonics **3**, 157 (2009).
13. J. Zuloaga and P. Nordlander, Nano Lett. **11**, 1280 (2011).
14. T. J. Davis, K. C. Vernon, and D. E. Gómez, J. Appl. Phys **106**, 043502 (2009).
15. S. A. Maier, P. G. Kik, H. A. Atwater, S. Meltzer, E. Harel, B. E. Koel, and A. A. Requicha, Nat. Mater. **2**, 229 (2003).
16. S. C. Yang, H. Kobori, C. L. He, M. H. Lin, H. Y. Chen, C. Li, M. Kanehara, T. Teranishi, and S. Gwo, Nano Lett. **10**, 632 (2010).
17. M. J. Guffey and N. F. Scherer, Nano Lett. **10**, 4302 (2010).
18. V. Myroshnychenko, J. Rodriguez-Fernandez, I. Pastoriza-Santos, A. M. Funston, C. Novo, P. Mulvaney, L. M. Liz-Marzan, and F. J. Garcia de Abajo, Chem. Soc. Rev. **37**, 1792 (2008).
19. U. Hohenester and J. Krenn, Phys. Rev. B **72**, 195429 (2005).
20. B. Xi, M. Qiu, S. Y. Xiao, H. Xu, and L. Zhou, Phys. Rev. B **89**, 035110 (2014).
21. S. Fan, W. Suh, and J. D. Joannopoulos, J. Opt. Soc. Am. A **20**, 569 (2003).
22. W. Suh, Z. Wang, and S. Fan, IEEE J. Quantum Electron. **40**, 1511 (2004).
23. L. Zhou, X. Huang, Y. Zhang, and S.-T. Chui, Mater. Today **12**(12), 52 (2009).
24. The parameters $\vec{p}$, $\vec{m}$ and $\langle\Phi|\Phi\rangle$ are calculated from numerical simulations based on the single-particle system.